Design and Demonstration of an Optical True-Time-Delay Device Based on an Octic-Style White Cell

Rashmi Mital, Carolyn M. Warnky, and Betty Lise Anderson, *Senior Member, IEEE*

***Abstract*—A methodology for designing an octic-style optical true-time-delay (TTD) device based on the White cell (WC) is investigated. The octic cell is a "polynomial" cell, one of the two classes of TTD White cells. This octic cell is designed to produce a maximum of 6399 delays in 17 bounces, with a unit delay of 3 ps. Glass blocks are used for short delays, white lens trains are used for the longer delays. The octic cell is designed to use a micro-electromechanical tip/tilt micromirror array to direct light beams into various delay paths.**

***Index Terms*—Array signal processing, beam steering, microelectromechanical devices, optical delay lines, optical signal processing, phased-array radar.**

I. Introduction

TRUE TIME delay (TTD) is a useful technique for enhancing the performance of phased array antennas (PAA) [1]. The use of phase shifters causes beam squint at different frequencies and inherently narrows the bandwidth of the antenna array [2]. In TTD devices, the timing of the arrival of the radio frequency (RF) signal is varied at the antenna elements to steer the radar beam [3]. TTD devices offer squint-free beam steering and wide bandwidths [4]–[8].

Compared to electrical TTD techniques, optical TTDs have advantages such as a natural resistance to electromagnetic interference, low weight, and low intrinsic losses [2]. To incorporate optical TTD, the RF signals are modulated onto light beams, which are then delayed by different times by varying the optical path. Many examples of optical TTD, including free-space delays and fiber delays, are described in literature [9]–[12]. Our TTD devices use free space.

We have been developing two types of architectures, both based on the White cell [13], called polynomial cells and exponential cells. In both cases, the optical beams experience multiple bounces m on some types of spatial light modulators (SLMs). In the polynomial cells, the number of sequential delays N is proportional to m raised to a power, where the power is determined by the structure of the cell. For example, the quadratic cell [14], [15] provides $N \propto m^2$ and the octic cell has $N \propto m^8$ [16]. In the exponential cells, the number of sequential delays is a base raised to a power determined by m. An example is the binary cell [16], [17] in which $N \propto 2^m$. Previously, we have reported on demonstrations of linear [19] and quadratic [14] cells.

The strength of the White-cell approach is not only that many delays can be produced but that many optical beams (hundreds) can circulate in the White cell at the same time; and thus, hundreds of antenna elements can be independently controlled with just a handful of hardware.

In this paper, we describe the design of an octic cell and the demonstration of a quartic cell, which is equivalent to half of an octic cell.

The organization of this paper is as follows. In Section II, we give a brief review of the White cell and its adaptation to polynomial cells. In Section III, we discuss the design of the octic cell including the layout, how the delays are implemented, the design procedure, and the final design of the octic cell. In Section IV, the experimental results will be presented. Finally, we summarize the research and draw conclusions in Section V.

II. White-Cell Overview

This section gives a brief overview of the White cell and how it can be adapted for polynomial cells. A detailed description of a polynomial cell based on the White cell is given elsewhere [14].

The White cell is a system of three spherical mirrors of identical radius of curvature, as shown in Fig. 1. An input beam is brought into the system via an input turning mirror located at the bottom of mirror M; and then, the beam bounces back and forth between the three mirrors, eventually walking off the top of mirror M. The mirrors A and B refocus the beam every round trip. Two imaging conditions need to be satisfied: mirrors A and B must image onto each other via mirror M and mirror M must image onto itself via either mirror A or mirror B with a magnification of -1.

With the refocusing characteristic of the White cell, a specific pattern of spots forms on the field mirror [14] that is determined by the location of the centers of curvature of mirrors A and B. This is also shown in Fig. 1, where the centers of curvature are marked. The focused spots are shown as circles and the corresponding numbers give the bounce number [14]. Two columns of spots form: one consisting of all even bounces and the other of odd bounces. Note that there can be many input beams; each traces out a unique spot pattern [14].

To adapt the White cell to true-time delay, we replace the field mirror, mirror M, with an equivalent flat mirror and a field lens. This combination reproduces the reflecting and

Manuscript received April 29, 2005; revised September 15, 2005.

R. Mital is with the Naval Research Lab, Washington, DC 20375 USA (e-mail: rmital@airborne.nrl.navy.mil).

C. M. Warnky and B. L. Anderson are with the Electrical Engineering Department, Ohio State University, Columbus, OH 43204 USA.

Digital Object Identifier 10.1109/JLT.2005.861912

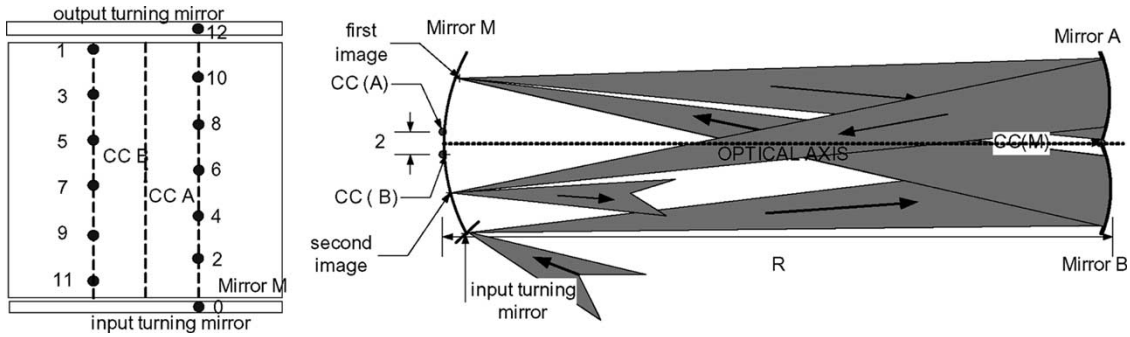

Fig. 1. Original White cell.

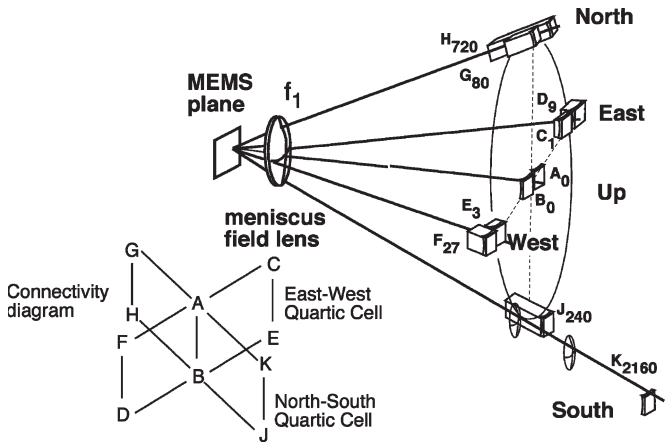

Fig. 2. Layout of the octic cell.

focusing functions of the field mirror. The flat-mirror equivalent is a microelectromechanical system (MEMS) device with micromirrors that can tilt in different directions. Because the light can be directed in multiple angles, we add optics in different directions to set up White cells of different lengths, all using the same MEMS device. For example, a two-position MEMS device was used in a linear cell [19], where $N \propto m$. In a quartic cell [18] with $N \propto m^4$, a three-state MEMS is required. The octic cell, where the number of delays is proportional to m^8, is made up of two quartic cells built in two perpendicular planes [18]. This cell requires a five-state MEMS and is described in more detail in the following section.

III. Design of the Octic Cell

A. Layout

The operation of the octic cell has been described in detail previously [18]. Briefly, the octic cell (Fig. 2) is a three-dimensional polynomial cell with ten arms, where an arm is defined as the path toward a spherical mirror, including any optic or delay elements along that path. Two arms in the same general direction are referred to as a wing, so there are five wings in the octic cell. The layout can be thought of as an east–west quartic cell combined with a north–south quartic cell. The MEMS device is located on the left-hand side of Fig. 2. This design of the octic cell contains a single field lens f_1 and ten spherical mirrors A–K. Arms C, D, E, and F each have a different optical path length and are part of the east–west quartic cell; while Arms G, H, J, and K, also of different lengths, are part of the north–south quartic cell. The null arms A and B are of the same length and are shared by both quartic cells.

In a White cell, beams bounce multiple times, being focused to a spot on each pass. Here, each spot lands on a different micromirror. The mirrors can be tipped to send a light beam that is coming from the null cell to any of the other four wings. If a beam from the null cell lands on a flat mirror, then the light stays in the null cell. Similarly, if the beam comes from the east wing, then a flat mirror sends it to the west wing and vice versa. The connectivity diagram in the lower left corner of Fig. 2 shows the possible transitions.

Each wing contains two spherical mirrors, of which one is to the left and the other is to right of the wing's axis. Arms A, D, E, H, and J are right arms; and B, C, F, G, and K are left arms. A light in the octic cell always alternates between left and right arms as it bounces.

The null arms of the octic cell have equal lengths and establish a minimum or bias delay that all beams experience. The other arms have longer lengths, which are all different. By selecting how many times each arm is visited by a beam during its m bounces in the octic cell, any delay in the sequence from 0 to $N\Delta$ can be obtained, where Δ is the time-delay increment. The increased path lengths can come from an extra distance in air, in dielectric blocks such as glass, or in a combination of both. Additional optics may be needed to satisfy the imaging conditions and constrain the diameter of the propagating beam. We discuss two different types of delay elements (glass blocks and lens trains) later in this section.

The equations for the delay assignment for the different delay arms are as follows. The derivations have been given previously [18].

$$
\begin{aligned}
C &\Rightarrow 1\Delta \\
E &\Rightarrow \left(\frac{m-1}{8}+1\right)\Delta = (\beta+1)\Delta \\
D &\Rightarrow [\beta+1]^2\Delta \\
F &\Rightarrow [\beta+1]^3\Delta \\
G &\Rightarrow [\beta^4+4\beta^3+6\beta^2+4\beta]\Delta \\
J &\Rightarrow [\beta^5+5\beta^4+10\beta^3+10\beta^2+4\beta]\Delta \\
H &\Rightarrow [\beta^6+6\beta^5+15\beta^4+20\beta^3+14\beta^2+4\beta]\Delta \\
K &\Rightarrow [\beta^7+7\beta^6+21\beta^5+35\beta^4+34\beta^3+18\beta^2+4\beta]\Delta \quad (1)
\end{aligned}
$$

where β is defined in the second line of (1).

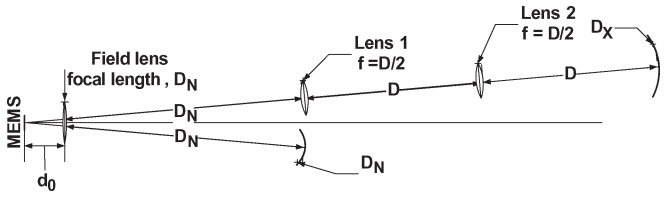

Fig. 3. Using a lens train for larger delays.

In (1), m is the number of times the beam hits MEMS micromirrors, which does not include input and output bounces, and Δ is the smallest delay unit. The maximum delay obtained from these delay arms is given by

$$N_{\mathrm{OCTIC}} = [\beta^8 + 8\beta^7 + 28\beta^6 + 56\beta^5 + 68\beta^4 + 48\beta^3 + 16\beta^2 + 0\beta - 1]. \quad (2)$$

To get the maximum delay, each of the arms is used β times except arms C and G, which are each visited one time fewer or $[\beta - 1]$ times.

B. Delay Implementation

We wish to provide delays ranging from a few picoseconds to a few nanoseconds. Each optically connected pair of arms must satisfy the two imaging conditions described earlier, regardless of the delay time. The delay requirements and imaging conditions can both be met simultaneously using blocks or lens trains. We discuss each type of delay element below.

1) Glass Blocks for Short Delays: We use glass blocks as delay elements for short delays. It takes the light longer to travel the same optical distance in glass as in air due to the increased refractive index n. Without the block, the distance d_1 between the field lens and the spherical mirrors must be equal to the focal length of the field lens. With the glass block present, the sum of the distance in air and the optical thickness of the glass block has to equal the focal length of the field lens [17].

For longer delays, the increased thickness of the blocks, whether glass or another dielectric material, may cause absorption loss to be a concern. Lens trains may be used for longer delays to reduce absorption loss.

2) Lens Trains for Longer Delays: Fig. 3 shows an example of a lens train used for a large delay. One wing is shown. For simplicity, the lower arm is shown as a simple White cell (WC) arm. Two lenses besides the field lens are added into the longer delay arm. The increased distance in air is $2D$, where D is the distance between a lens and the following optical element, giving a delay of $2D/c$ seconds compared to the null case. In this type of lens train, lens 1 is conjugate to the White-cell mirrors (mirrors X and N) and lens 2 is conjugate to the MEMS device. For very long delays, it may be necessary to use several pairs of lenses to ensure that the beam does not become too large due to divergence.

It is possible to adjust the positions and focal lengths of the lenses such that the image of the MEMS forms in between lens 1 and lens 2, instead of at lens 2. We can then use this real image plane for input and output turning mirrors, rather than placing them in the actual MEMS plane.

TABLE I
DELAYS AND RELATIVE DISTANCES FOR EACH DELAY ARM OF THE OCTIC CELL

ARM	Delay (ps)	Distance in Air Relative to Null Arm (mm)
C	3	0.45
E	9	1.35
D	27	4.05
F	81	12.15
G	80	36.00
J	240	108.00
H	2160	324.00
K	6480	972.00

We used a design rule of $f/10$ paraxial optics to minimize aberrations. This requirement limits the minimum delay that can be implemented in a lens train.

C. Design Procedure

The steps in the design procedure are as follows. First, we decide whether each arm will contain a glass block or lens train based on the delay specifications. Next, we determine the beam spot size on the MEMS. Then, we define the optical layout of the two null arms and the eight delay arms using the two imaging conditions and the required time delays. These parameters include the focal lengths of any lenses, the distances between optical elements, the thickness of any blocks, and the radii of curvature of the objective mirrors. The final step is to calculate the diameter of each optical component.

1) Specifications: The specifications for our TTD cell are: a wavelength of 1.55 μm, a minimum delay Δ of 3 ps, and the number of sequential delays N of 1000 or more. Using (1), the relative delays for a 17-bounce octic-cell system are as shown in the second column of Table I. For these delays, the increased free-space distances (over the optical path in the null arms) are tabulated. Note that in the octic cell, 17 bounces produce 6399 different delays. If the number of bounces were reduced to the next integer value of β (which would be $\beta = 1$), the number of delays would be only 224 and does not meet our specification of at least 1000. In this case, we get many extra delays for free.

We chose to use glass blocks for seven of the eight delay arms and a lens train for the longest arm. Except for arm K, all arms have spherical mirrors of the same radius of curvature. To use standard off-the-shelf lenses and to satisfy the $f/10$ conditions in the longest arm, we compromised and designed arm K to give a delay of 6783 ps instead of 6480 ps for a proof-of-concept demonstration.

2) Spot Size: The beam spot size on the MEMS pixel influences loss and the overall size of the TTD cell. If the spots are large, then they may be truncated by the MEMS pixels; resulting in power loss and diffraction. If the spots are small then beam divergence is high, requiring larger optics to contain the beam. Assuming a Gaussian beam, the far-field half-angle divergence is

$$\theta_{\mathrm{div}} = \frac{\lambda}{\pi w_0} \quad (3)$$

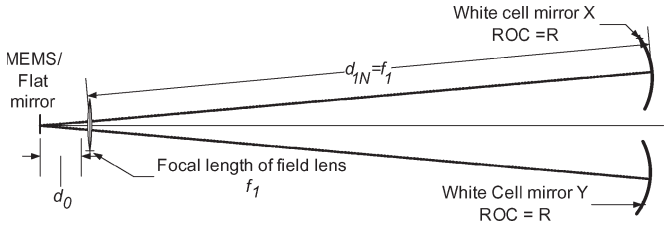

Fig. 4. General null cell.

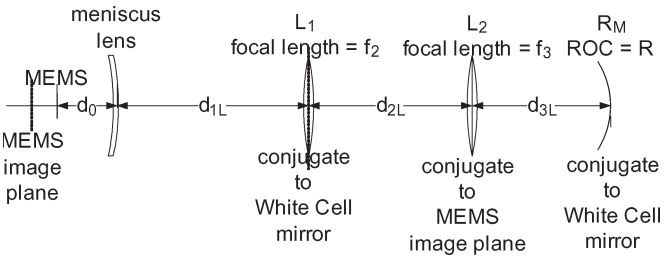

Fig. 5. Lens train used for long delays.

where λ is the wavelength and w_0 is the spot size, defined as the beam radius where the field is e^{-1} of the peak. To capture more than 99.99% of the power of a Gaussian beam on a square MEMS pixel, we set the spot size w_0 to be 1/4 of the side of the pixel. For example, for a pixel that is 100 μm on a side, our spot size is 25 μm in ($1/\mathrm{e}$ field) radius.

3) Null Cell: The design process begins with the null cell. The wing shown in Fig. 4 may be considered to be a general null cell. The MEMS device is on the left-hand side. The field lens of focal length f is located at a distance of d_0 from the MEMS device. The two White-cell (or objective) mirrors are each placed at an equal distance d_{1N} from the field lens, measured along the axis of the arm. For simplicity, we treat each arm as a centered system, allowing us to use paraxial ray matrices.

Generally, we begin by choosing d_0, calculating the required diameter of the field lens, and then choosing f_1 to satisfy our $f/\#$ design rule. The imaging conditions then set distance d_{1N} equal to the focal length of the field lens f_1 and independent of the distance d_0 [16]. The radius of curvature R of the White-cell mirror R_X and R_Y is given by

$$R = \frac{d_{1N}^2}{d_{1N} - d_0} = \frac{f_1^2}{f_1 - d_0}. \tag{4}$$

The null cell is complete.

4) Arm With Delay Block: Next, we consider an arm with a delay block. The distance to the field lens d_0 and focal length f_1 of the field lens are already fixed (same lens as the null arm). We have to solve for the distance in air d_{1G}, the thickness of the glass block d_{2G}, and the radius of curvature R of the White-cell mirror. These can be determined by three equations, one from the required delay and two from the imaging conditions. Using the first imaging condition, the relationship of d_{1G} and d_{2G} to f_1 is given by [16]

$$f_1 = d_{1G} + \frac{d_{2G}}{n}. \tag{5}$$

The radius of curvature R of the White-cell mirror can be solved in terms of f_1 and d_0 using the second imaging condition

$$R = -\frac{\left(d_{1G} + \frac{d_{2G}}{n}\right)^2}{d_0 - \left(d_{1G} + \frac{d_{2G}}{n}\right)} = -\frac{f_1^2}{d_0 - f_1}. \tag{6}$$

To solve for the distances in air and glass, we consider the desired time delay ΔT [18], which is twice the time difference between one pass through the delay arm and one pass through the null arm. The distance d_{1G} represents the distance between the field lens and the White-cell mirror that is in air, and d_{2G} represents the length of the glass. The distances d_{1G} and d_{2G} in the delay arms can then be determined from

$$\left[\frac{d_{1G}}{c} + \frac{d_{2G}}{\frac{c}{n}}\right] - \left[\frac{d_{1N}}{c} + \frac{d_{2N}(=0)}{\frac{c}{n}}\right] = \frac{\Delta T}{2}$$

$$(d_{1G} - d_{1N}) + n d_{2G} = \frac{\Delta T}{2} c. \tag{7}$$

To simplify the equation, it can be assumed that the glass block in the null arm has zero thickness.

Since d_{1N} and f_1 are known, (5) and (7) can be used to determine d_{1G} and d_{2G}. Finally, R can be determined using (6).

5) Arm With Lens Train: Now let us go through the design of a lens train as represented in Fig. 5. In this figure, the field lens is shown as a meniscus lens, which was chosen to reduce aberrations.

Recall from Section III-B that L_1 is conjugate to the WC mirror of the null arm. This makes the distance d_{1L} equal to the focal length of the field lens. Lens L_2 images L_1 onto the White-cell mirror. This determines the focal length of lens L_2. Distances d_{2L} and d_{3L} are equal and are determined by the required delay. The focal length of lens L_1 can be determined using the fact that lens L_1 forms an image of the MEMS device on the plane of lens L_2. The final White-cell mirror images L_2 back onto itself, so the radius of curvature R is equal to d_{3L}. Using these steps, we can determine all the unknown variables in the lens-train arm.

However, for our design, we made some changes since we wanted to use off-the-shelf lenses in the lens train. Instead of having d_{1L} equal to f_1, we placed lens L_1 closer to the field lens. We also did not require that the delay obtained from the lens train be exactly equal to the theoretical delay. Finally, the image of the MEMS formed somewhere in between lens 1 and 2 rather than at lens 2.

6) Diameters: Once all the focal lengths and the distances between the various components have been determined in terms of the field lens' focal length, the next step is to determine the diameters of the components. The diameters depend on the divergence angle of the beam, the overall size of the MEMS device, and the angles between the arms of the different wings of the octic cell.

The angle ψ between the two arms of any wing is shown in Fig. 6. The angle ψ is set by how close the White-cell mirrors can be, which in turn is determined by the size of the beam at the White-cell mirrors.

Fig. 6 also shows that the field lens bends the optical axes of the arms. This has to be considered when calculating the

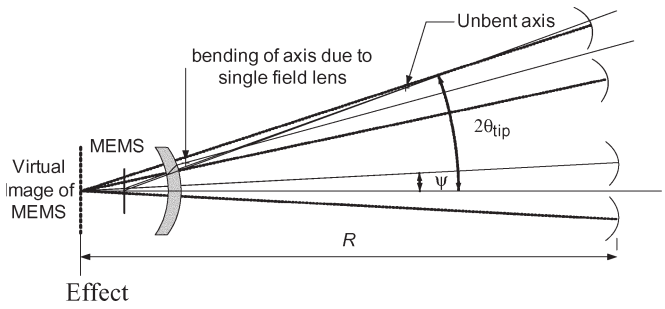

Fig. 6. Effect of refraction due to single field lens on $\theta_{\rm tip}$ and ψ.

diameter of the field lens. The angle between the central axes of two wings is $2\theta_{\rm tip}$.

To determine the value of the angle ψ, we first determine the diameter of the White-cell mirrors from the divergence angle of the beam and the distances between the field lens and the White-cell mirror (d_{1N} for the null arm). We assume the White-cell mirrors in a wing are touching each other. The diameter ϕ of the White-cell mirror is related to the $1/{\rm e}$ field divergence half angle of the beam $\theta_{\rm div}$, a quantity we will call the divergence factor $\varepsilon_{\rm div}$, and the distance d_{1N} by

$$\begin{aligned}\phi &= 2 \times (\text{radius of WC mirror}) \\ &= 2 \times \left[d_{1N} \times (\varepsilon_{\rm div} \times \tan(\theta_{\rm div}))\right]. \end{aligned} \tag{8}$$

Here ε_{div} is a design factor that ensures that lenses are large enough such that a negligible beam truncation occurs. To choose ε_{div}, we consider the ratio of the power P captured by a given circular optical element and the total power P_{Total} for a Gaussian beam

$$\begin{aligned}\frac{P}{P_{\rm TOTAL}} &= 1 - {\rm e}^{-\frac{2r^2}{w^2}} \\ &= 1 - {\rm e}^{-2(\varepsilon_{\rm div})^2} \end{aligned} \tag{9}$$

where r is the radius of the circular WC mirror or field lens and w is the radius of the beam on the mirror or lens. For 99.9% of the power to be contained, $\varepsilon_{\rm div}$ has to be 1.858. We made $\varepsilon_{\rm div}$ equal to 3.0 to be conservative and to ensure that 100% of the power was constrained on the surface of the lens.

The angle between the arms can then be found from

$$\tan \Psi = \left(\frac{\phi}{2R}\right). \tag{10}$$

Once Ψ has been determined, we can use Ψ, $\theta_{\rm div}$ and $\theta_{\rm tip}$ to determine the final diameter of the field lens by

$$\begin{aligned}\text{Lens Diameter} &= 2 \times \text{radius of field lens} \\ &= 2 \times d_0 \left[\tan(2\theta_{\rm tip} + 3\theta_{\rm div} + \psi)\right] + a \end{aligned} \tag{11}$$

where d_0 is the distance between the MEMS device and the field lens and a is the height of the MEMS device.

Fig. 7 represents the role of each term in (11) in determining the diameter of the field lens. The figure shows a close-up view of the MEMS device and the field lens. Rays from the MEMS device are shown for the outermost angles and for the center angles. Each beam is shown as a cone to depict the divergence of the beam.

7) MEMS Tip Angle Accuracy: It is a characteristic of White-cell devices that they do not require that the angle of the MEMS device be extremely accurate [20]. The purpose of the MEMS device is only to select which White-cell mirror the beam is directed toward. IF the MEMS tilt angle is off a little, the spot will not be perfectly centered on the White-cell mirror. Increasing the diameter of the White-cell mirrors slightly can compensate any inaccuracy in the MEMS device. On the other hand, there is a need to accurately align the White-cell mirrors since they image one pixel onto another, but this needs to be done only once.

D. Final Design

The final design for the octic cell is now presented. Table II shows the distances in each arm, in millimeters, and the thicknesses of the delay blocks made of BK7 glass. Note that while no blocks are technically required in the null arms A and B, we added a 6-mm bias to those arms (and added 6 mm to the other blocks) to prevent having to manufacture blocks of large area but very small thickness.

Table III gives the radii of curvature for each optical surface and the diameters of the optics.

This completes the design of the octic cell. This TTD device works on a free-space approach and provides small delays using glass blocks and large delays using lens trains. In the next section, we present the results of a proof-of-concept experimental demonstration using four of the eight delay arms.

IV. Experimental Results

We built a "quartic" cell to demonstrate the basic principles of the octic cell. This consists of three wings (six arms) arranged all in the east–west plane. To demonstrate both long and short delays, we kept arms C and D of the original east–west cell (delays of $\Delta = 3$ ps and $9\Delta = 27$ ps); and then, added arms J $(240\Delta = 720$ ps) and K (6783 ps, an approximation to 2160Δ as mentioned in Section III-C from the original north–south plane).

The experimental layout of the experiment is shown in Fig. 8. The MEMS device is located on the left-hand side of the figure with the field lens immediately to the right. Because the lengths of the arms do not give a range of consecutive delays, it is not a true quartic cell. In addition, due to availability and time constraints, we used 50.8-mm diameter White-cell mirrors instead of 101.6-mm mirrors. The resulting loss can be easily corrected in future implementations. The drawing is scaled.

In the figure, arm K is quite long, so it has been broken up for clarification. In arm K, the plane where the image of the MEMS forms is shown. This is where the input and output turning mirrors are located.

A. Input and Output Optics

We used a single optical beam to demonstrate operation of the system. The input comes from a fiber-pigtailed laser (Princeton Lightwave, A011711A-AT-034) with the single

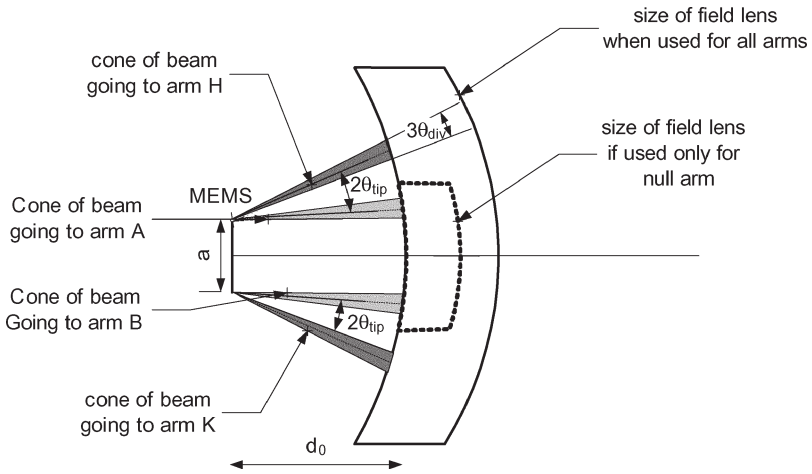

Fig. 7. Determining the size of field lens.

TABLE II
DISTANCE (IN MILLIMETERS) IN THE OCTIC CELL

Arm	d_0 (mm)	d_{1G} (mm)	d_{2G} (mm)
A/B	24.97	705.45	6.00
C	24.97	705.14	6.54
E	24.97	702.21	7.62
D	24.97	704.37	10.86
F	24.97	695.73	20.58
G	24.97	676.65	49.20
J	24.97	619.05	135.6
H	24.97	446.25	394.8
K	24.97	609.45	d_2=679.4 d_3=443.1

TABLE III
OPTICAL PARAMETERS AS DESIGNED (IN MILLIMETERS)

Optical Element	R_1 Radii of Curvature	R_2 Radii of Curvature	t thickness	ϕ, diameter
Field lens	-47	-50	12.5	60
Lens train L_1	308.5	-308.5	8.3	50.8
Lens train L_2	256.8	-256.8	8.3	50.8
Mirrors (A-J)	-750	--	--	101.6
Mirror K	-600	--	--	50.8

mode fiber producing a beam radius of approximately 5 μm. Our spot size at the MEMS plane and the image plane needs to be 25 μm, so we magnified the input by a factor of five [Fig. 9(a)]. We used 20$\times$ and 4$\times$ microscope objectives back to back to produce the magnification. A right-angle prism was placed at the image plane to reflect the beam into the TTD cell.

A similar setup is used to reflect the output spot to a photodetector, as shown in Fig. 9(b). In the experiment, the output spot size was closer to 100 μm than the intended 25 μm, due to truncation and the resulting diffraction at the White-cell mirrors (recall we used smaller mirrors than required). The photodetector is a New Focus 1417, whose active radius is 10 μm. We demagnified the output spot by a factor of two, again accomplished with microscope objectives. The demagnified spot still overfills the photodetector.

Fig. 10(a) shows a schematic view of a MEMS device with a bounce pattern of ten bounces. Our MEMS device is Calient Diamondwave half switch [21]. The micromirrors have continuously variable tilt angles but we are using them in either the flat state or tipped at $\pm 10^\circ$. The centers of curvature of all the even mirrors (mirrors B, K, and C) are located at one location while the centers of curvature of all the odd mirrors (mirrors A, D, and J) are also superimposed. Then, as the beam travels between even and odd mirrors, it returns to the correct pixel regardless of the particular path chosen. The connectivity chart in Fig. 10(b) shows that the beam has to alternate between even and odd mirrors, similar to the left and right mirrors of the octic cell.

B. Results

To measure the delays, we use a configuration as shown in the block diagram of Fig. 11. A frequency-swept RF signal from port 1 of a network analyzer (an Agilent E8362B) modulates the light beam via a Mach-Zehnder modulator (JDS Uniphase Model AM-150). The RF signal from the photodetector is brought into port 2 of the network analyzer and the S_{21} parameter is measured. An internal Fourier transform in the network analyzer results in a displayed response in the time domain. We reference the measurements to the case where every bounce is in the null cell and measure the relative delays of the other paths.

Fig. 12 shows some sample delay measurements for (a) the time delay for the null arm and (b) for one trip to Arm J. The latter delay is produced by turning pixels 3 and 4 to -10°, so that the beam goes through Arm J instead of Arm A on one trip through the cell. In the figure, the vertical scale is 20 dB/div and the horizontal scale ranges from -6.0 ns to $+6.0$ ns.

The measured delays of all the arms are given in Table IV. This table also lists the amount of tuning that was done in each arm. Each arm was aligned and focused as well as possible using IR cards and cameras. Final tuning was done using the delay measurement on the network analyzer. For example, initial measurements showed that arm C was measuring a delay

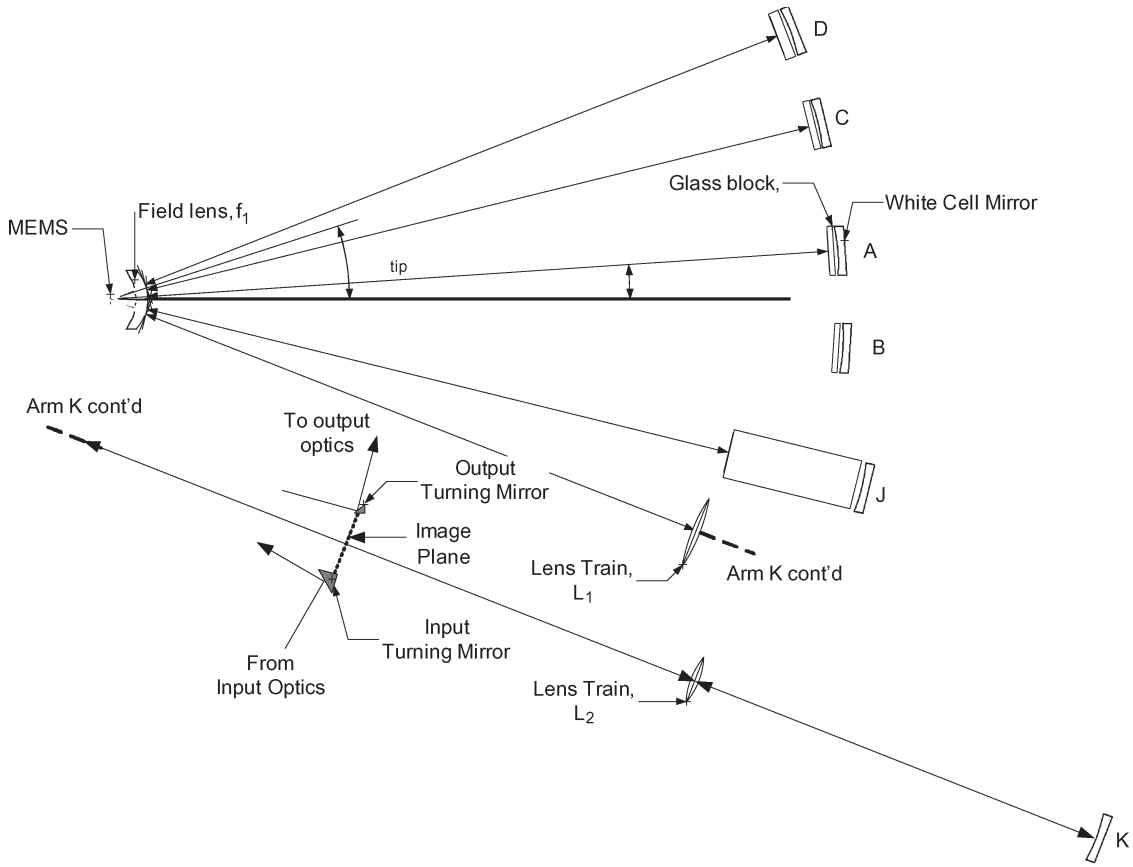

Fig. 8. Layout of the "quartic" cell experiment.

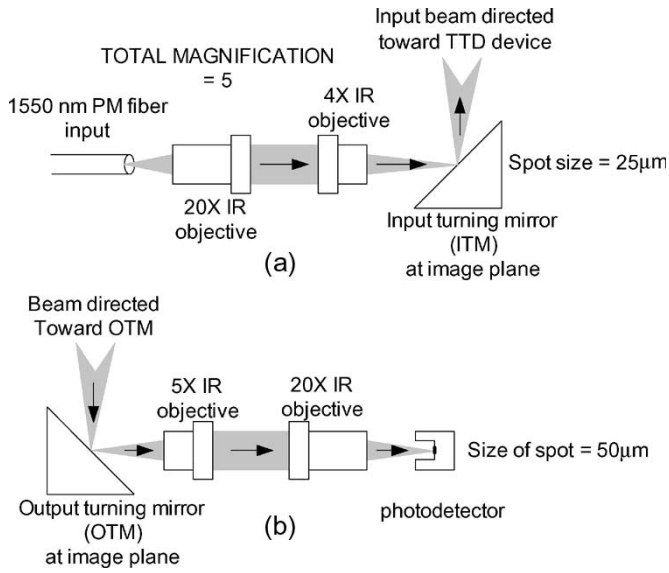

Fig. 9. (a) Input optics and (b) output optics.

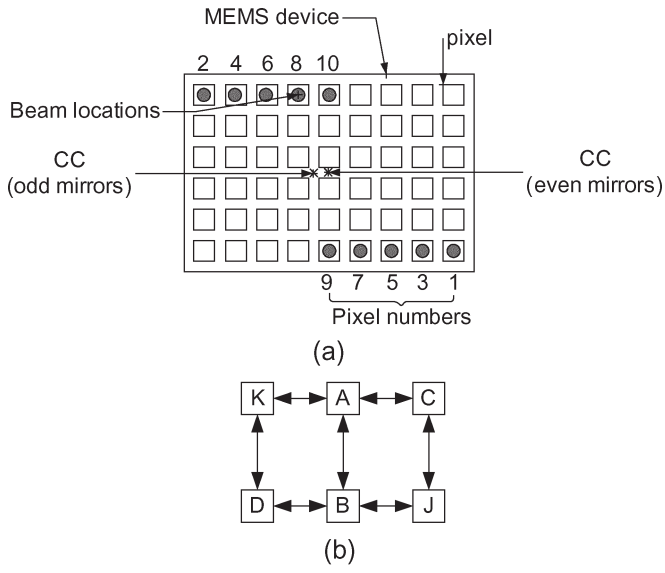

Fig. 10. (a) Bounce pattern on MEMS device and (b) connectivity between the arms.

of 10 ps, which was off by 7 ps. By translating the WC mirror, we were able to fix the delay to the designed value. In the physical system, the lengths of the arms with glass blocks can be tuned by changing the z-position of the White-cell mirrors.

We were not able to tune arm J to the required delay since we ran out of travel on the translation stage holding mirror J. This problem can be fixed by relocating the position of mirror J, which we did not go back to and do because of time constraints.

Arm K had a similar problem in the setup. In this case, getting the right delay involved repositioning and realigning all of the lenses in the lens train. This is a harder realignment problem compared to the previous case. The position of the lenses in the lens train also affects the position of the image plane. Thus, any change in the location of the lenses would involve realigning the input optics. Since the aim of this research is to prove that we

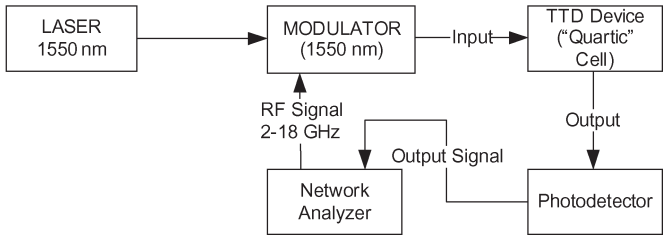

Fig. 11. Block diagram for delay measurements.

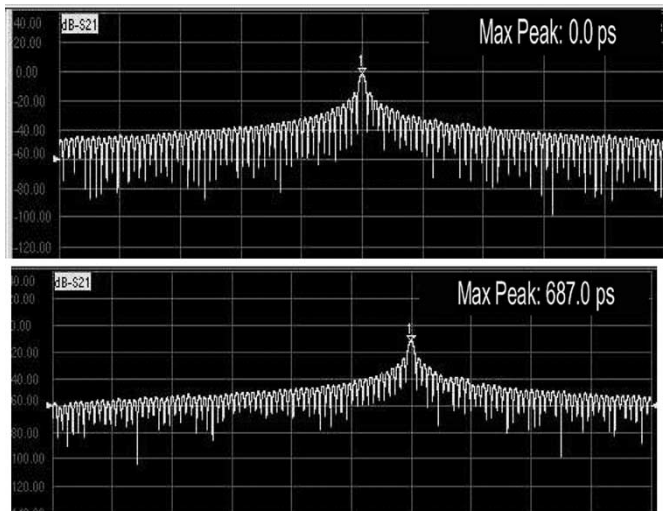

Fig. 12. (a) Time delay calibrated to ten bounces in the null wing and (b) time taken to travel to arm J once.

TABLE IV
MEASURED TIME DELAYS FOR SINGLE ARMS

Mirror Pattern	Delay Goal (ps)	Measured Delay (+/- 0.5)ps	Tuned By (+/- 0.5)
Null	0.0	0.0	0.0
C	3.0	3.0	7.0
D	27.0	27.0	3.0
J	720.0	687.0	--
K	6783.0	7053.0	--

are able to bounce a beam back and forth between the different delay arms as well as measure delays from the various arms, no more time was spent in fixing the delays to obtain exact theoretical delays.

Table V shows the delays for various combinations of arms. In this table, the expected delay column is the time delay expected given the actual experimental delays of each of the arms individually. The maximum delay obtained is by one visit to each different delay arm.

V. SUMMARY AND CONCLUSION

In this paper, we have reported a demonstration of switchable time delays in a polynomial White-cell-based optical true-time-delay device from a minimum of 3 ps to more than 7.5 ns with an accuracy of 0.5 ps. The true-time-delay device comprises multiple White cells of different lengths, all sharing a three-position MEMS micromirror array.

TABLE V
MEASURED TIME DELAYS FROM "QUARTIC" CELL

Mirror Pattern	Expected Delay (ps)	Measured Delay (in ps +/- 0.5 ps)
C twice	6.0	6.0
D twice	54.0	54.0
J twice	1374.0	1374.0
C+D	30.0	30.0
D+J	714.0	714.0
D+J+C	717.0	717.0
K+D	7080.0	7080.0
C+J+K+D	7770.0	7770.0

The complete octic cell is three-dimensional with ten arms in two orthogonal planes, eight of which provide delay. The delay comes from a free-space travel in air and glass blocks, with a lens train in one arm to contain the size of the beam. As a proof-of-concept, we built six of the ten arms of the octic cell, two of the shortest arms from the east–west cell, and two of the longest arms from the north–south cell. We measured time delays in the cell and found that we could tune them up to 7 ps without loss of focus.

The device that we demonstrated experimentally is a subset of the octic cell. This demonstration shows that it is possible to build a high-order polynomial cell with the use of a tilting micromirror device.

ACKNOWLEDGMENT

The authors would like to thank S. A. Collins, Jr. for the discussions, especially during the designing of the glass blocks and the lens trains delay elements.

REFERENCES

[1] W. Ng, A. A. Walston, G. L. Tangonan, J. J. Lee, I. L. Newberg, and N. Bernstein, "The first demonstration of an optically steered microwave phased array antenna using true time delay," *J. Lightw. Technol.*, vol. 9, no. 9, pp. 1124–1131, Sep. 1999.

[2] P. J. Mathews and R. D. Esman, "Cascading prism dispersion [Phased array antennas]," *IEEE Potentials*, vol. 18, no. 5, pp. 13–15, Jan. 2000.

[3] H. Zmuda and E. N. Toughlian, "Photonic aspects of modern radar," in *The Artech House Optoelectronics Library*, B. Culshaw, A. Rogers, and H. Taylor, Eds. Norwood, MA: Artech House, 1994.

[4] E. N. Toughlian and H. Zmuda, "A photonic variable RF delay line for phased array antennas," *J. Lightw. Technol.*, vol. 8, no. 12, pp. 1824–1828, Dec. 1990.

[5] M. Clenet, "Visualization of the array factor of phased arrays using time delay units and digital phase shifters," in *Proc. Antennas and Propagation Society Int. Symp.*, San Antonio, TX. Piscataway, NJ: IEEE Press, Jun. 16–21, 2002, vol. 1, pp. 520–523.

[6] T. Takahashi, Y. Konishi, and K. Hariu, "Error analysis for phased array antennas with true time delay modules," in *Proc. Antennas and Propagation Society Int. Symp.*, San Antonio, TX. Piscataway, NJ: IEEE Press, Jun. 16–21, 2002, vol. 1, pp. 606–609.

[7] D. T. K. Tong and M. C. Wu, "Multiwavelength optically controlled phased array antennas," *IEEE Trans. Microw. Theory Tech.*, vol. 46, no. 1, pp. 108–115, Jan. 1998.

[8] Z. F. R. Li and R. T. Chen, "Compact broadband 5-bit photonic true time delay module for phased array antennas," *Opt. Lett.*, vol. 23, no. 7, pp. 522–524, Apr. 1998.
[9] N. Madamopoulos and N. A. Riza, "Demonstration of an all digital 7-bit 33-channel photonic delay line for phased array antennas," *Appl. Opt.*, vol. 39, no. 23, pp. 4168–4181, Aug. 2000.
[10] E. G. Paek, Y. S. Im, J. K. Choe, and T. K. Oh, "Acoustically steered and rotated true time delay generator based on wavelength division multiplexing," *Appl. Opt.*, vol. 39, no. 8, pp. 1298–1308, Mar. 2000.
[11] M. Y. Frankel and R. D. Esman, "Reconfigurable time steered array antenna beam former," *Appl. Opt.*, vol. 36, no. 35, pp. 9261–9268, Dec. 1997.
[12] B. Tsap, Y. Chang, H. R. Fetterman, A. F. J. Levi, D. A. Cohen, and I. Newberg, "Phased-array optically controlled receiver using a serial feed," *IEEE Photon. Technol. Lett.*, vol. 10, no. 2, pp. 267–269, Feb. 1998.
[13] J. White, "Long optical paths for large aperture," *J. Opt. Soc. Amer.*, vol. 32, no. 5, pp. 285–288, May 1942.
[14] B. L. Anderson, S. A. Collins, Jr., E. A. Beecher, C. A. Klein, and S. B. Brown, "Optically produced true-time delays for phased array antenna arrays," *Appl. Opt.*, vol. 36, no. 32, pp. 8493–8503, Nov. 1997.
[15] B. L. Anderson and C. D. Liddle, "Optical true time delay for phased array antennas: Demonstration of a quadratic White cell," *Appl. Opt.*, vol. 41, no. 23, pp. 4912–4921, Aug. 2002.
[16] R. Higgins, N. K. Nahar, and B. L. Anderson, "Design and demonstration of a switching engine for a binary true-time delay device that uses a White cell," *Appl. Opt.*, vol. 42, no. 23, pp. 4747–4757, Aug. 2003.
[17] S. Kunathikom, B. L. Anderson, and S. A. Collins, "Design and delay elements in a binary optical true-time delay device that uses a White cell," *Appl. Opt.*, vol. 42, no. 35, pp. 6984–6994, Dec. 2003.
[18] B. L. Anderson and R. Mital, "Polynomial-based optical true-time delay devices with microelectromechanical mirror arrays," *Appl. Opt.*, vol. 41, no. 26, pp. 5449–5461, Sep. 2002.
[19] A. Radar and B. L. Anderson, "Demonstration of a linear true-time delay device by use of a microelectromechanical mirror array," *Appl. Opt.*, vol. 42, no. 8, pp. 1409–1416, Mar. 2003.
[20] X. Zheng, V. Kaman, S. Yuan, Y. Xu, O. Jerphagnon, A. Keating, R. C. Anderson, H. N. Poulsen, B. Liu, J. R. Sechrist, C. Pusarla, R. Helkey, D. J. Blumenthal, and J. E. Bowers, "Three-dimensional MEMS photonic cross-connect switch design and performance," *IEEE J. Sel. Topics Quantum Electron.*, vol. 9, no. 2, pp. 571–578, Mar./Apr. 2003.
[21] B. L. Anderson *et al.*, "Optical cross-connect switch based on tip/tilt micromirrors in a White cell," *IEEE J. Quantum Electron.*, vol. 9, no. 2, pp. 579–593, Mar./Apr. 2003.

Rashmi Mital received the B.Eng. degree from Nanyang Technological University, Singapore, in 1998 and the M.S. and Ph.D. degrees from The Ohio State University, Columbus, in 2001 and 2005, respectively, all in electrical engineering. Her Ph.D. dissertation was in the development of a true time delay (TTD) based on a recirculating (White) cell and micromirror technology.

She is currently with the Naval Research Lab, Washington, DC, and is the author of a paper in applied optics.

Carolyn M. Warnky received the B.S. degree in electronic engineering from Southern Illinois University-Edwardsville, in 1979 and the M.S. and Ph.D. degrees in electrical engineering from The Ohio State University, Columbus, in 1994 and 2002, respectively.

She is a Post-Doctoral Researcher at The Ohio State University.

Dr. Warnky is a member of the Optical Society of America (OSA).

Betty Lise Anderson (S'75–M'79–SM'95) received the B.S. in electrical engineering at Syracuse University, Syracuse, NY, in 1978 and the M.S. and Ph.D. degrees in materials science and electrical engineering at the University of Vermont, Burlington, in 1988 and 1990, respectively.

She spent nine years in the industry including Tektronix, Inc., GTE Laboratories, and Draper Laboratories. She is currently a Professor at the Department of Electrical and Computer Engineering, The Ohio State University, Columbus. Her current research interests include analog optical signal processing, devices for optical communication systems, coherence, and semiconductor devices. She is the coauthor (with R. L. Anderson) of *Fundamentals of Semiconductor Devices* (Burr Ridge, IL: McGraw Hill, 2005).

Prof. Anderson is a member of the Optical Society of America (OSA). She is the Associate Editor for IEEE JOURNAL OF QUANTUM ELECTRONICS.